Accepted Manuscript



Enhanced 1-butylamine gas sensing characteristics of flower-like V_2O_5 hierarchical architectures

Tianye Yang, Hai Yu, Bingxin Xiao, Zhifang Li, Mingzhe Zhang

PII: S0925-8388(17)30039-7

DOI: 10.1016/j.jallcom.2017.01.028

Reference: JALCOM 40395

To appear in: *Journal of Alloys and Compounds*

Received Date: 9 November 2016

Revised Date: 19 December 2016

Accepted Date: 3 January 2017

Please cite this article as: T. Yang, H. Yu, B. Xiao, Z. Li, M. Zhang, Enhanced 1-butylamine gas sensing characteristics of flower-like V_2O_5 hierarchical architectures, *Journal of Alloys and Compounds* (2017), doi: 10.1016/j.jallcom.2017.01.028.

This is a PDF file of an unedited manuscript that has been accepted for publication. As a service to our customers we are providing this early version of the manuscript. The manuscript will undergo copyediting, typesetting, and review of the resulting proof before it is published in its final form. Please note that during the production process errors may be discovered which could affect the content, and all legal disclaimers that apply to the journal pertain.

ACCEPTED MANUSCRIPT

Enhanced 1-butylamine gas sensing characteristics of flower-like V_2O_5 hierarchical architectures

Tianye Yang, Hai Yu, Bingxin Xiao, Zhifang Li and Mingzhe Zhang*

*State key laboratory of Superhard materials, Jilin University, Changchun 130012, People's Republic of China.

Correspondence and requests for materials should be addressed to zhangmz@jlu.edu.cn

ACCEPTED MANUSCRIPT

ACCEPTED MANUSCRIPT

Abstract

Vanadium oxide hierarchical architectures have been successfully synthesized using a facile hydrothermal method. The as-prepared V_2O_5 hierarchical architectures are assembled by nanobelts and present a unique radial flower-like morphology. The as-prepared V_2O_5 hierarchical structures are used for organic polluted and toxic gas 1-butylamine gas detection. The gas sensors based on V_2O_5 hierarchical architectures present excellent 1-butylamine gas sensing performances. Such as a fast response time (9 s), high sensitivity, good selectivity and superior repeatability, all these properties are predominantly-attributed to the unique nanobelt-assembled radial flower-like structure and ammonium ions intercalation. The obtained V_2O_5 hierarchical architectures will hold promising potential in the fabrication of efficient and effective 1-butylamine gas sensors for practical applications.

Keywords: V_2O_5; hierarchical architectures; 1-butylamine; gas sensor

ACCEPTED MANUSCRIPT

1. Introduction

For the past few years, all countries around the world are facing atmospheric environmental problems which have become one of the most serious issues [1]. Gas sensitive materials have been attracted intense interest and extensively investigated in sensor application [2, 3]. Among a variety of gas sensitive materials, metal oxide semiconductors (MOS) have been extensively investigated. They are usually recognized as the most economic materials as gas sensors, such as high sensitivity, fast response and recovery, low detection limits, low fabrication cost, simplicity in fabrication, measurement, and function durability compared to other semiconductors [4]. For example, SnO_2 [5], ZnO [6], In_2O_3 [7], NiO [8], WO_3 [9], CuO [10], CeO_2 [11] and TiO_2 [12, 13] are very common MOS and widely applied in various gas detection. Vanadium oxide, as an n-type semiconductor with a band gap of 2.2 eV, has received large amounts of attention in the past few years. It can be applied in wide fields, such as lithium battery electrode [14, 15], supercapacitors [16], selective catalytic reduction catalyst [17] and gas sensors [18-21], etc. Especially, V_2O_5 hierarchical architecture materials have been widely reported such as V_2O_5 nanorods self-assembled hollow V_2O_5 microspheres [22], V_2O_5 hierarchical microspheres [23], self-organized spherical nano-urchins [24] and nanoplates packed flower-like V_2O_5 microspheres [25], etc. Such hierarchical structures usually possess a large surface area which can provide plenty of active sites. The diffusion and favorable paths for the effective reaction of the examined gas are also provided by the hierarchical architectures. These hierarchical structural characteristics are in favor of the adsorption and desorption of the detected gas [26]. Therefore, controllable synthesis of desired composition is crucial to achieve high-performance gas sensors.

1-butylamine, as an industrial common organic agent, has been widely applied in many fields such as insecticides, pharmaceuticals, dyes, textiles, steel corrosion inhibitor and plasma-polymerization applications [27-31]. People have benefitted from its extensive application in industry, however, it is polluted, toxic and harmful for human health and environment [32]. Moreover, 1-butylamine is extremely

flammable and corrosive as well. Hence, it is essential to develop a high performance gas sensor to realize the rapid detection of 1-butylamine for any unexpected leakage. However, there are seldom studies done on industrial organic polluted gas 1-butylamine.

Herein, our interest is in controlling morphology and structure of V_2O_5 for gas sensing motivated by their affinity to organic amines [33], especially 1-butylamine [34]. We focus on fabricating hierarchical architectures with highly designed structural characteristics which can be potential for gaining high performance 1-butylamine sensors. In this paper, flower-like V_2O_5 hierarchical architectures are successfully synthesized by a facile hydrothermal method. The obtained V_2O_5 hierarchical architectures are assembled by a number of nanobelts and present radial flower-like morphology. Furthermore, the as-fabricated V_2O_5 hierarchical architectures based sensors exhibit high sensitivity and fast response time (9 s) characteristic to 1-butylamine, holding great potential as a high-performance sensing material for detecting organic toxic gas 1-butylamine.

2. Experimental section

2.1 Synthesis of flower-like V_2O_5 hierarchical structures

All reagents (analytical-grade purity) were used as purchased without further purification. The synthesis of flower-like V_2O_5 hierarchical structures was carried out by a typical hydrothermal method. The first procedure, 0.117g ammonium metavanadate (NH_4VO_3) and 0.125 g polyvinylpyrrolidone (PVP) were dissolved in 18 ml deionized water under magnetic stirring for 10 min at room temperature. Then, 2 ml oxalic acid aqueous was put (0.5 M) into the prepared solution and kept stirring for 2 h at room temperature to form a light green solution. Subsequently, the mixed solution was transferred to a Teflon-lined, stainless-steel autoclave with a 50 ml capacity, maintained at 180 ^oC for 4 h. After cooling down to room temperature naturally, the dark blue precipitate were collected and washed with deionized water and anhydrous alcohol for three times respectively by centrifugalization, and dried at 60 ^oC in air. At last, the flower-like V_2O_5 hierarchical architectures were obtained by

calcining the precipitates at 350 ^{o}C for 2 h and then 400 ^{o}C for 30 min in air in turn. The heating rate was controlled at 3 ^{o}C min^{-1}.

2.2 Material characterization

The as-prepared products were characterized by Rigaku D/max-2500 X-ray powder diffraction (XRD) with Cu-Ka1 radiation (λ = 1.54056 Å) at a scanning rate of 4° min^{-1}. Field-emission scanning electron microscopy (FESEM) images were obtained by using a Magellan 400 FEI microscope operating at 2 kV. The transmission electron microscopy (TEM), and high resolution TEM (HRTEM) images were performed on a JEOL JEM-2200FS microscope. The elemental composition and chemical state of the products were investigated by X-ray photoelectron spectroscopy (XPS) (ESCALAB MK II). The diffuse reflectance UV-visible spectrum of the sample was recorded using a UV-visible-near infrared spectrophotometer. The properties of the gas sensor were carried out by a CGS-8 intelligent gas sensing analysis system. The sensor response was defined as S = R_a/R_g [35]. Here, R_a and R_g were the resistances of the sensors in the air and target gas, respectively. The response and recovery time was defined as the time taken by the sensors to achieve 90 % of the total resistance change in the case of adsorption and desorption, respectively.

3. Results and discussion

3.1 Morphology and composition analysis

The as-synthesized sample was mixed with deionized water to form a paste. The paste was coated on a ceramic tube on where a pair of gold electrodes was printed beforehand and each electrode was connected with two Pt wires. A Ni–Cr heating wire was inserted into the tube to form an indirect-heated sensing device. The structure of the sensor is shown in Fig. 1. The as-prepared gas sensing device is stabilized at a constant temperature for 12 h to fully evaporate water and make ceramic tube and the sample contact closely. After the water is evaporated completely, the V_2O_5 thin film morphology is maintained on the ceramic tube, which is shown in the FESEM image in the inset of Fig. 1.

The X-ray diffraction patterns of flower-like V_2O_5 hierarchical architectures are

illustrated in Fig. 2. Each indices of lattice plane have been labelled. It can be seen that the diffraction peaks are consistent with JCPDS Card Files No. 86-2248 and the V_2O_5 hierarchical architectures have an orthorhombic structure. The strong and sharp peaks indicate that the crystallized samples are well ordered. Furthermore, no diffraction peaks derived from any other impurities can be detected, which indicates the high purity of the sample.

The morphology and structure characterization of the flower-like V_2O_5 hierarchical architectures are investigated by using the scanning electron microscopy (SEM) and the transition electron microscope (TEM). The typical morphology and size of the obtained V_2O_5 products are revealed by FESEM. The low magnification SEM images from Fig. 3a and b clearly illustrate that the sample is composed of abundant flower-like structures with sizes from 5 to 7 μm. Moreover, no other morphologies can be detected indicating a high uniformity of the product. Enlarged SEM image of an individual flower-like hierarchical V_2O_5 architectures is shown in Fig. 3c and d, the flower-like V_2O_5 is assembled by a mass of nanobelts which are tightly stacked together. Numerous belt-shaped nanobranches are connected into one center disk and radially arranged to form a flower-like morphology.

To further investigate detailed morphology and structure of the samples, the TEM and HRTEM analysis are carried out. Fig. 4a illustrates a typical TEM image of an individual V_2O_5 hierarchical architectures, from which we can observe that the sample are approximate circle shape and the inner parts are solid, further confirming the regular flower-like hierarchical structures. Additionally, the diameter of the single specific unit of the V_2O_5 sample is about 6 μm, which is in agreement with the results from the SEM analysis. As shown in Fig. 4b, it is clearly to find that the hierarchical structures are constitutive of nanobelts from the edge of the sample. Fig. 4c shows the HRTEM image of the nanobelts which assembles the flower-like V_2O_5 hierarchical architectures. The interplanar distances of the fringes are measured and found to be 0.34 nm which agree well with the spacing of the (101) planes for the orthorhombic structure (JCPDS Card no. 86-2248).

To investigate the surface chemical composition, the corresponding XPS V 2p and

O 1s spectra are carried out and shown in Fig. 5. The V 2p 3/2 at 517.5 eV shows a single peak which corresponds to vanadium species in the oxidation state +5 [36]. For O 1s, the main peak is located at 530.3 eV which can be assigned to O^{2-} [37]. The spin–orbit split of V 2p 3/2 and V 2p1/2 is around 7.6 eV, which is quite consistent with the previous literatures [38, 39]. The energy difference between the binding energy of the O 1s level and that of V 2p 3/2 is about 12.8 eV, which is quite consistent with the reported values of pure V_2O_5 material [40], indicating that a full V_2O_5 stoichiometry is indeed present in the as-prepared sample.

3.3 Optical properties

The UV-vis absorption spectrum of the V_2O_5 hierarchical architectures are clarified and illustrated in Fig. 6a. It is clearly seen that the peak in the UV region is observed at a wavelength of around 384 nm. The strong absorption in the UV region is attributed to band gap absorption in V_2O_5. The band-gap value can be calculated by the following equation:

$$(\alpha h\upsilon)^{n} = A\,(h\upsilon - Eg) \quad (1)$$

where α, h, υ, A and E_g are indicative of the absorption coefficient, Planck's constant, light frequency, constant value, and band-gap energy, respectively [41]. For the V_2O_5 material, the n value is 1/2 for the indirect band-gap semiconductor. The plot of $(\alpha h\upsilon)^{1/2}$ versus hυ is shown in the Fig. 6b, and the band-gap value (E_g) around 2.48 eV was calculated by estimating the intercept of the tangent to the curve. The obtained Eg is larger than that of bulk V_2O_5 (~2.2 eV) [38]. The obtained E_g value suggests that the as-prepared sample contains nanostructures, which is corresponding to nanobelts obtained from SEM and TEM results. The nanobelts hold large specific surface area which favors enhancing gas sensing properties.

3.4 Gas sensing properties

V_2O_5 hierarchical architectures assembled by numerous individual nanobelts are very promising due to their large effective surface area and great surface activity, which make them ideal candidates for gas sensing materials. The morphologies of the synthesized sample after sensor fabrication and heat treatment are shown in Fig. S1 in

the supplementary materials it can be observed that the morphology of the samples has no obvious change. In the gas sensing study, the operating temperature is an important parameter for the investigation on gas sensing properties due to its great influence on the surface state of sensing materials, as well as the contact reactions during the gas sensing process. Each sensor has an optimum operating temperature, at which the sensor exhibits the highest response to the targeted gases. The flower-like V_2O_5 hierarchical architectures are tested for sensitivity to 100 ppm 1-butylamine to determine the optimum working temperature. As shown in Fig. 7a, it can be observed that all response curves of the sensors exhibit a parabola-shape with the raise of temperature in the range of 100 to 180 ^oC. The response of V_2O_5 sensor reaches to the maximum with temperature up to 140 ^oC and then rapidly decreases with a further increase in temperature. Thus, 140 ^oC is chosen as the optimum working temperature for further investigation of the as-prepared gas sensor. The lower working temperature may be ascribed to the more active sites on the V_2O_5 surfaces [20, 42].

It has been widely accepted that gas sensors for practical applications are required high response as well as excellent selectivity to the targeted gases. Hence, the responses of the V_2O_5 sensor to 100 ppm benzene (C_6H_6), toluene (C_7H_8), ammonia (NH_3), and methanol (CH_3OH) at the optimum operating temperature of 140 ^oC are measured to investigate the selectivity of the sensor. As shown in Fig. 7b, the V_2O_5 sensor shows much higher sensitivity to 1-butylamine than to benzene, toluene, ammonia and methanol, indicating the superior selectivity of the V_2O_5 sensor.

Stability, that is, the ability to successively respond to a target gas without a visible decrease in sensor response, is another important feature of a sensor. The long-term stability and repeatability of the as-prepared sensor are investigated by measuring the 1-butylamine with a concentration of 100 ppm at optimum operating temperature 140 ^oC. As shown in Fig. 8a, it can be observed that the average response is 2.6 with a concentration of 100 ppm 1-butylamine, revealing that the sensor can be reused and there is no obvious change in the response amplitude. Moreover, within the 4 cycles, the sensor still maintains fast response and recovery state. Fig. 8b illustrates that the response time and recovery time of the hierarchical structures to 100 ppm of

1-butylamine is as short as 9 and 49 s, respectively. The resistance decreases rapidly on injection of 1-butylamine and then rapidly recovers to the initial value after the gas is released, indicating a good response-recovery behavior. The dynamic response curve of the as-fabricated gas sensor to different concentrations of 1-butylamine (10–100 ppm) at 140 ^{o}C is shown in Fig. 8c. And Fig 8c illustrates the reproducibility of the flower-like V_2O_5 sensor, revealing that the sensor maintains its initial response amplitude without a clear decrease upon five successive sensing tests to various concentrations of 1-butylamine and also indicates a detection limit of 10 ppm. In addition, the response of the sensor changes rapidly when exposed to 1-butylamine and to air, indicating the excellent reproducibility. These results indicate that the sensor based on the flower-like V_2O_5 hierarchical architectures exhibits excellent gas sensing properties.

A comparison between the sensing performances of the flower-like V_2O_5 based sensors and literature reports is summarized in Table 1. It is noteworthy that although the response value of the sensor based on V_2O_5 hierarchical architectures is not the highest, the optimum working temperature (140 ^{o}C) is lower than some literature reports. In addition, the rapid response time (9 s) and recovery time (49 s) show the advantage of V_2O_5 hierarchical structures in comparison with ZnO/Au nanoflakes [43], $Ag_2V_4O_{11}$ [44], and V_2O_5 nanofibers [34].

3.5 Gas sensing mechanism

The electron depletion theory has been widely used to explain the gas sensing mechanism by the chemical adsorption and reaction of gas molecules on the surface of the sensing materials [45, 46]. In ambient environment, typical n-type metal oxide semiconductors such as V_2O_5 shows a conductance change owing to the mass of oxygen absorbed. The change in resistance is caused by the adsorbed O_2 trapping electrons from the conduction band of the nanocrystals. In the present system, when the sensor is set in air, the oxygen molecules are adsorbed on the surface of nanobelts and capture the electrons from the V_2O_5 hierarchical architectures surface to form adsorbed oxygen ions, such as O_2^- and O^- (mainly O^- at 140 ^{o}C) [47], which result in

the decrease of the conductance of the sensor. When the sensor is exposed to 1-butylamine gas, the adsorbed oxygen ions react with the adsorbed 1-butylamine molecules and release the trapped electrons to conduction band, which increases the conductance of the V_2O_5 sensor. The enhanced 1-butylamine gas sensing performances of V_2O_5 flower-like hierarchical architectures can be explained by two aspects. On the one hand, nanobelt-assembled flower-like hierarchical architectures can facilitate the diffusion of the oxygen and test gases, increasing the utilization rate of the sensing body. Moreover, nanobelt-assembled hierarchical architectures can provide more surface active sites available for the gas sensing reaction and better electron mobility, which is improving gas sensing properties. On the other hand, the enhanced gas sensing performances can be attributed to the effect of ammonium ions intercalation. Raible et al. [34] suggest that the change of conductance of V_2O_5 nanofibers induced by organic amine may be attributed to not only the adsorption onto the fiber but also the intercalation of amine molecules into the layered structures, because the intercalation of alkyl ammonium ions can significantly increase the distance between the oxide layers [33]. Thus, electron transfer from the 1-butylamine to the V_2O_5 layered structure becomes easier and then results in the increase of conductance of the hierarchical architectures, which further enhances gas sensing properties. Therefore, the excellent gas sensing performance of flower-like V_2O_5 hierarchical architectures can be attributed to the cooperative sensitization effect of unique nanobelt-assembled radial flower-like architectures and ammonium ions intercalation.

Conclusions

To sum up, flower-like V_2O_5 hierarchical architectures are successfully synthesized by a facile hydrothermal method. The as-prepared V_2O_5 samples are assembled by numerous nanobelts and present radial flower-like hierarchical structure morphologies. The V_2O_5 hierarchical architectures sensor exhibits a superior sensitivity and fast response (9 s) towards 100 ppm 1-butylamine at the optimum working temperature of 140 ^oC. The excellent 1-butylamine gas sensing performance can be mainly attributed to the cooperative sensitization effect of unique nanobelt-assembled radial flower-like

structure and ammonium ions intercalation. It is expected that vanadium oxide gas sensors would be a good choice for detecting organic toxic gas 1-butylamine.

Acknowledgements

This work was funded by the National Science Foundation of China, Nos. 11474124, 61674065 and Specialized Research Fund for the Doctoral Program of Higher Education of China, No. 20130061110012.

ACCEPTED MANUSCRIPT

References

[1] C.K. Chan, X. Yao, Air pollution in mega cities in China, Atmospheric Environment, 42 (2008) 1-42.

[2] J.H. Lee, Gas sensors using hierarchical and hollow oxide nanostructures: Overview, Sensor Actuat B-Chem, 140 (2009) 319-336.

[3] J. Li, X. Liu, J. Cui, J. Sun, Hydrothermal synthesis of self-assembled hierarchical tungsten oxides hollow spheres and their gas sensing properties, ACS Appl Mater Interfaces, 7 (2015) 10108-10114.

[4] E. Comini, G. Faglia, G. Sberveglieri, Z.W. Pan, Z.L. Wang, Stable and highly sensitive gas sensors based on semiconducting oxide nanobelts, Applied Physics Letters, 81 (2002) 1869-1871.

[5] Y. Wei, C. Chen, G. Yuan, S. Gao, SnO_2 nanocrystals with abundant oxygen vacancies: Preparation and room temperature NO_2 sensing, Journal of Alloys and Compounds, 681 (2016) 43-49.

[6] H. Bian, S. Ma, A. Sun, X. Xu, G. Yang, S. Yan, J. Gao, Z. Zhang, H. Zhu, Improvement of acetone gas sensing performance of ZnO nanoparticles, Journal of Alloys and Compounds, 658 (2016) 629-635.

[7] F. Li, J. Jian, R. Wu, J. Li, Y. Sun, Synthesis, electrochemical and gas sensing properties of In_2O_3 nanostructures with different morphologies, Journal of Alloys and Compounds, 645 (2015) 178-183.

[8] X. San, G. Wang, B. Liang, J. Ma, D. Meng, Y. Shen, Flower-like NiO hierarchical microspheres self-assembled with nanosheets: Surfactant-free solvothermal synthesis and their gas sensing properties, Journal of Alloys and Compounds, 636 (2015) 357-362.

[9] J. Sun, J. Guo, J. Ye, B. Song, K. Zhang, S. Bai, R. Luo, D. Li, A. Chen, Synthesis of Sb doping hierarchical WO_3 microspheres and mechanism of enhancing sensing properties to NO_2, Journal of Alloys and Compounds, 692 (2017) 876-884.

[10] S. Bhuvaneshwari, N. Gopalakrishnan, Enhanced ammonia sensing characteristics of Cr doped CuO nanoboats, Journal of Alloys and Compounds, 654 (2016) 202-208.

[11] Z. Li, X. Niu, Z. Lin, N. Wang, H. Shen, W. Liu, K. Sun, Y.Q. Fu, Z. Wang, Hydrothermally synthesized CeO_2 nanowires for H_2S sensing at room temperature, Journal of Alloys and Compounds, 682 (2016) 647-653.

[12] P.X. Zhao, Y. Tang, J. Mao, Y.X. Chen, H. Song, J.W. Wang, Y. Song, Y.Q. Liang, X.M. Zhang, One-Dimensional MoS_2-Decorated TiO_2 nanotube gas sensors for efficient alcohol sensing, Journal of Alloys and Compounds, 674 (2016) 252-258.

[13] X. Zhao, W. Shi, H. Mu, H. Xie, F. Liu, Templated bicontinuous Tin oxide thin film fabrication and the NO_2 gas sensing, Journal of Alloys and Compounds, 659 (2016) 60-65.

[14] D. Fang, L. Li, W. Xu, G. Li, Z. Luo, C. Liang, Y. Ji, J. Xu, C. Xiong, Self-assembled hairy ball-like V_2O_5 nanostructures for lithium ion batteries, RSC Advances, 4 (2014) 25205-25209.

[15] F. Guo, M. Fan, P. Jin, H. Chen, Y. Wu, G.-D. Li, X. Zou, Precursor-mediated synthesis of double-shelled V_2O_5 hollow nanospheres as cathode material for lithium-ion batteries, CrystEngComm, (2016).

[16] J.S. Bonso, A. Rahy, S.D. Perera, N. Nour, O. Seitz, Y.J. Chabal, K.J. Balkus Jr, J.P. Ferraris, D.J. Yang, Exfoliated graphite nanoplatelets–V_2O_5 nanotube composite electrodes for supercapacitors, Journal of Power Sources, 203 (2012) 227-232.

[17] F. Hernandez-Ramirez, J.D. Prades, R. Jimenez-Diaz, T. Fischer, A. Romano-Rodriguez, S. Mathur, J.R. Morante, On the role of individual metal oxide nanowires in the scaling down of chemical sensors, Physical Chemistry Chemical Physics, 11 (2009) 7105-7110.

[18] W. Jin, S. Yan, L. An, W. Chen, S. Yang, C. Zhao, Y. Dai, Enhancement of ethanol gas sensing response based on ordered V_2O_5 nanowire microyarns, Sensors and Actuators B: Chemical, 206 (2015)

284-290.

[19] R. Wang, S. Yang, R. Deng, W. Chen, Y. Liu, H. Zhang, G.S. Zakharova, Enhanced gas sensing properties of V_2O_5 nanowires decorated with SnO_2 nanoparticles to ethanol at room temperature, RSC Advances, 5 (2015) 41050-41058.

[20] Y.T. Wang, W.T. Whang, C.H. Chen, Hollow V_2O_5 Nanoassemblies for high-performance room-temperature hydrogen sensors, ACS Appl Mater Interfaces, 7 (2015) 8480-8487.

[21] W. Yan, M. Hu, D. Wang, C. Li, Room temperature gas sensing properties of porous silicon/V_2O_5 nanorods composite, Applied Surface Science, 346 (2015) 216-222.

[22] A. Dhayal Raj, T. Pazhanivel, P. Suresh Kumar, D. Mangalaraj, D. Nataraj, N. Ponpandian, Self assembled V_2O_5 nanorods for gas sensors, Current Applied Physics, 10 (2010) 531-537.

[23] S.A. Hakim, Y. Liu, S. Yang, G.S. Zakharova, W. Chen, Synthesis and Ethanol sensing properties of V_2O_5 hierarchical microspheres, Ferroelectrics, 477 (2015) 77-83.

[24] C. O'Dwyer, D. Navas, V. Lavayen, E. Benavente, M.A. Santa Ana, G. González, S.B. Newcomb, C.M. Sotomayor Torres, Nano-Urchin: The Formation and Structure of High-Density Spherical Clusters of Vanadium Oxide Nanotubes, Chemistry of Materials, 18 (2006) 3016-3022.

[25] A. Dhayal Raj, P. Suresh Kumar, Q. Yang, D. Mangalaraj, Synthesis and gas sensors behavior of surfactants free V_2O_5 nanostructure by using a simple precipitation method, Physica E: Low-dimensional Systems and Nanostructures, 44 (2012) 1490-1494.

[26] J. Li, X. Liu, J. Cui, J. Sun, Hydrothermal synthesis of self-assembled hierarchical tungsten oxides hollow spheres and their gas sensing properties, ACS Applied Materials & Interfaces, 7 (2015) 10108-10114.

[27] K. Kim, J.W. Lee, D. Shin, J.-Y. Choi, K.S. Shin, Organic isocyanide-adsorbed gold nanostructure: a SERS sensory device for indirect peak-shift detection of volatile organic compounds, Analyst, 137 (2012) 1930-1936.

[28] F. Paraguay D, M. Miki-Yoshida, J. Morales, J. Solis, W. Estrada L, Influence of Al, In, Cu, Fe and Sn dopants on the response of thin film ZnO gas sensor to ethanol vapour, Thin Solid Films, 373 (2000) 137-140.

[29] J.M. BASTIDAS, J.D. DAMBORENEA, A.J. VA´ZQUEZ, Butyl substituents in n-butylamine and their influence on mild steel corrosion inhibition in hydrochloric acid, Journal of Applied Electrochemistry, 27 (1997) 345-349.

[30] Z. Wu, Y. Yan, G. Shen, R. Yu, A novel approach of antibody immobilization based on n-butyl amine plasma-polymerized films for immunosensors, Analytica Chimica Acta, 412 (2000) 29-35.

[31] I. Gancarz, G. Poźniak, M. Bryjak, W. Tylus, Modification of polysulfone membranes 5. Effect of n-butylamine and allylamine plasma, European Polymer Journal, 38 (2002) 1937-1946.

[32] X. Ding, K.-L. Yang, Liquid crystal based optical sensor for detection of vaporous butylamine in air, Sensors and Actuators B: Chemical, 173 (2012) 607-613.

[33] A. Bouhaouss, P. Aldebert, Intercalation d'ions alkylammonium et d'alkylamines a longues chaines dans les gels de V_2O_5, Materials Research Bulletin, 18 (1983) 1247-1256.

[34] I. Raible, M. Burghard, U. Schlecht, A. Yasuda, T. Vossmeyer, V_2O_5 nanofibres: novel gas sensors with extremely high sensitivity and selectivity to amines, Sensors and Actuators B: Chemical, 106 (2005) 730-735.

[35] S. Park, H. Kim, D. Kim, Growth and fabrication method of CdTe and its performance as a radiation detector, Journal of the Korean Physical Society, 66 (2015) 31-36.

[36] C.W. Zou, Y.F. Rao, A. Alyamani, W. Chu, M.J. Chen, D.A. Patterson, E.A.C. Emanuelsson, W. Gao,

ACCEPTED MANUSCRIPT

Heterogeneous lollipop-like V_2O_5/ZnO array: A promising composite nanostructure for visible light photocatalysis, Langmuir, 26 (2010) 11615-11620.

[37] R. Suresh, K. Giribabu, R. Manigandan, S. Munusamy, S. Praveen Kumar, S. Muthamizh, A. Stephen, V. Narayanan, Doping of Co into V_2O_5 nanoparticles enhances photodegradation of methylene blue, Journal of Alloys and Compounds, 598 (2014) 151-160.

[38] M. Benmoussa, E. Ibnouelghazi, A. Bennouna, E.L. Ameziane, Structural, electrical and optical properties of sputtered vanadium pentoxide thin films, Thin Solid Films, 265 (1995) 22-28.

[39] A.Z. Moshfegh, A. Ignatiev, Formation and characterization of thin film vanadium oxides: Auger electron spectroscopy, X-ray photoelectron spectroscopy, X-ray diffraction, scanning electron microscopy, and optical reflectance studies, Thin Solid Films, 198 (1991) 251-268.

[40] C.W. Zou, X.D. Yan, J. Han, R.Q. Chen, W. Gao, Microstructures and optical properties of β-V_2O_5 nanorods prepared by magnetron sputtering, Journal of Physics D: Applied Physics, 42 (2009) 145402.

[41] B. Liu, X. Li, Q. Zhao, J. Liu, S. Liu, S. Wang, M. Tade, Insight into the mechanism of photocatalytic degradation of gaseous o-dichlorobenzene over flower-type V_2O_5 hollow spheres, Journal of Materials Chemistry A, 3 (2015) 15163-15170.

[42] J. Cui, L. Shi, T. Xie, D. Wang, Y. Lin, UV-light illumination room temperature HCHO gas-sensing mechanism of ZnO with different nanostructures, Sensors and Actuators B: Chemical, 227 (2016) 220-226.

[43] Y.V. Kaneti, X. Zhang, M. Liu, D. Yu, Y. Yuan, L. Aldous, X. Jiang, Experimental and theoretical studies of gold nanoparticle decorated zinc oxide nanoflakes with exposed {1 0 0} facets for butylamine sensing, Sensors and Actuators B: Chemical, 230 (2016) 581-591.

[44] H. Fu, X. Yang, X. Jiang, A. Yu, Silver vanadate nanobelts: A highly sensitive material towards organic amines, Sensors and Actuators B: Chemical, 203 (2014) 705-711.

[45] Y. Shen, T. Yamazaki, Z. Liu, D. Meng, T. Kikuta, N. Nakatani, M. Saito, M. Mori, Microstructure and H_2 gas sensing properties of undoped and Pd-doped SnO_2 nanowires, Sensors and Actuators B: Chemical, 135 (2009) 524-529.

[46] Q. Wan, Q.H. Li, Y.J. Chen, T.H. Wang, X.L. He, J.P. Li, C.L. Lin, Fabrication and ethanol sensing characteristics of ZnO nanowire gas sensors, Applied Physics Letters, 84 (2004) 3654-3656.

[47] A.L. Zou, Y. Qiu, J.J. Yu, B. Yin, G.Y. Cao, H.Q. Zhang, L.Z. Hu, Ethanol sensing with Au-modified ZnO microwires, Sensors and Actuators B: Chemical, 227 (2016) 65-72.

ACCEPTED MANUSCRIPT

ACCEPTED MANUSCRIPT

Figure Captions

Fig. 1 Schematic image of the V_2O_5 sensor and SEM image (inset) of the as-prepared V_2O_5 sample.

Fig. 2 XRD patterns of the flower-like V_2O_5 hierarchical structures.

Fig. 3 FESEM images of the V_2O_5 hierarchical structures: (a–b) low magnification; (c–d) high magnification.

Fig. 4 (a) The low magnification TEM image, (b) the enlarged TEM and (c) the HRTEM of flower-like V_2O_5 hierarchical structures.

Fig. 5 XPS core level spectra of flower-like V_2O_5 hierarchical structures.

Fig. 6 (a) UV-vis absorption spectrum of flower-like V_2O_5 hierarchical structures. (b) The plot of the corresponding plot of $(\alpha h\upsilon)^{1/2}$ vs. photon energy ($h\upsilon$).

Fig. 7 (a) Responses of the flower-like V_2O_5 hierarchical structures to 100 ppm 1-butylamine at different operating temperatures, and (b) responses of the sensor upon exposure to 100 ppm various testing gases.

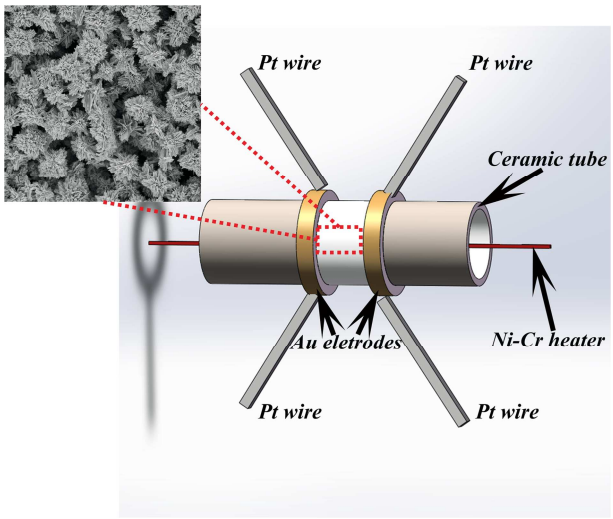
Fig. 8 (a) Response and recovery repeatability curve to 100 ppm 1-butylamine at 140 ^oC, (b) the transient response exhibition to 100 ppm 1-butylamine of the sensor at 140 ^oC and (c) the dynamic response of V_2O_5 sensors to different 1-butylamine concentrations (10-100 ppm) at 140 ^oC.

Table 1. Comparison of the 1-butylamine sensing performance of as-synthesized V_2O_5 hierarchical structures against previously various reported metal oxide nanostructures.

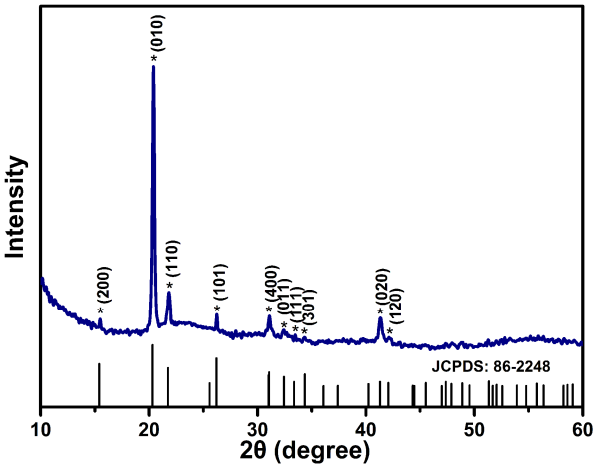
ACCEPTED MANUSCRIPT

Sample	1-butylamine (ppm)	Response (S = R_a/R_g)	τ_{res}/τ_{rec} (s)	Operating Temp. (^oC)	Ref.
ZnO/Au nanoflakes	100	73.2	37/47	240	31
$Ag_2V_4O_{11}$ nanobelts	50	3.5	-/-	260	32
V_2O_5 nanofibers	10	0.42	-/-	22	27
V_2O_5 hierarchical nanostructures	100	2.6	9/49	140	This work

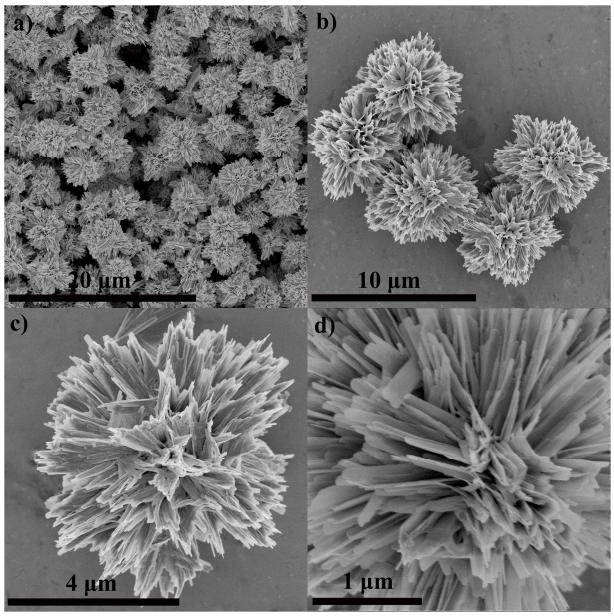
ACCEPTED MANUSCRIPT



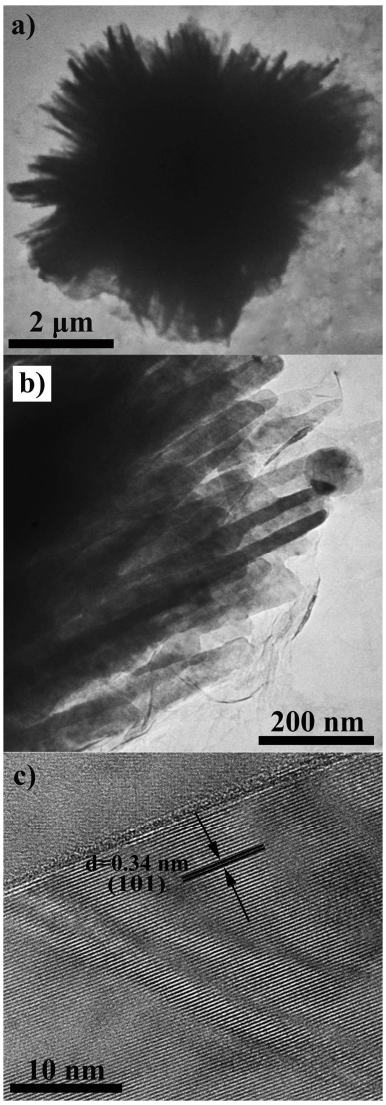
ACCEPTED MANUSCRIPT



ACCEPTED MANUSCRIPT

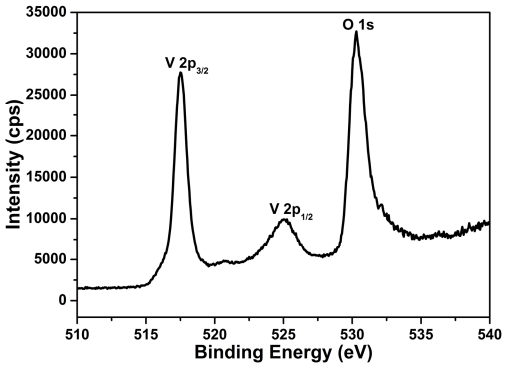


ACCEPTED MANUSCRIPT



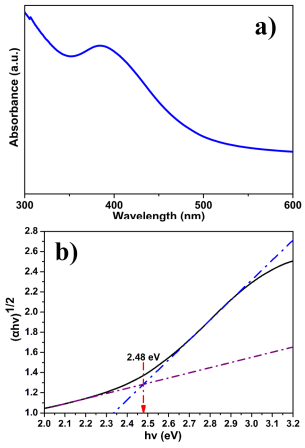
ACCEPTED MANUSCRIPT

ACCEPTED MANUSCRIPT

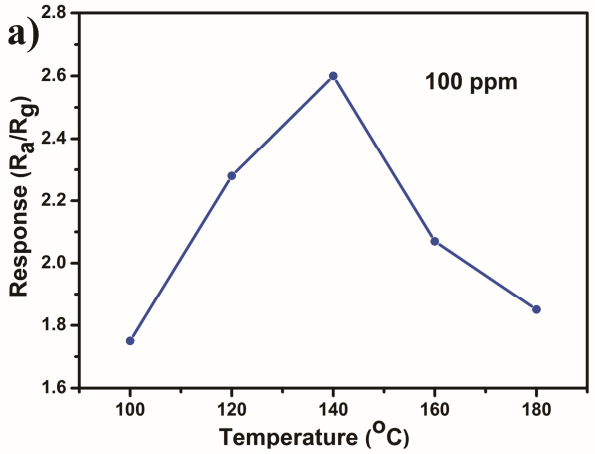


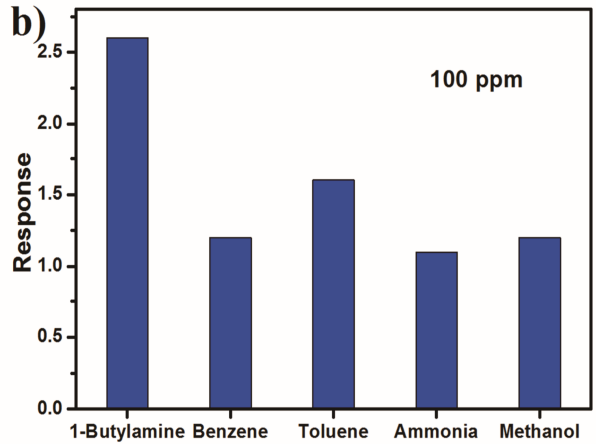
ACCEPTED MANUSCRIPT

ACCEPTED MANUSCRIPT

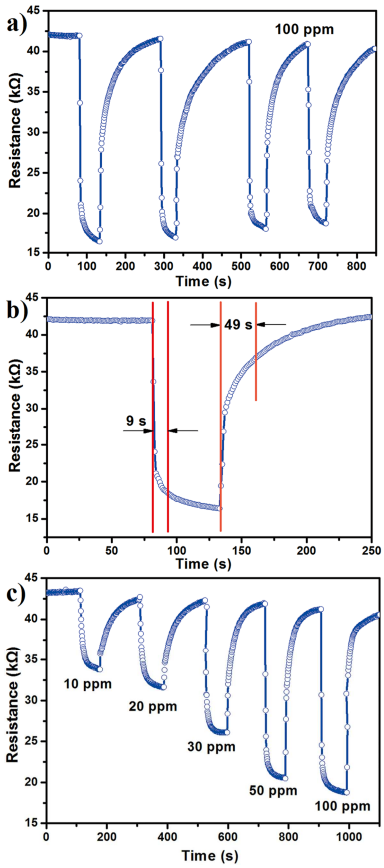


ACCEPTED MANUSCRIPT





ACCEPTED MANUSCRIPT



ACCEPTED MANUSCRIPT

ACCEPTED MANUSCRIPT

1. Hierarchical V_2O_5 architectures were synthesized by a facile hydrothermal process.
2. The as-prepared V_2O_5 sensor showed enhanced sensing properties to 1-butylamine.
3. The gas sensing mechanism of the V_2O_5 sensor was discussed in detail.

ACCEPTED MANUSCRIPT